



## Degree-1 convection in the Martian mantle and the origin of the hemispheric dichotomy

James H. Roberts<sup>1</sup> and Shijie Zhong<sup>2</sup>

Received 16 December 2005; revised 7 March 2006; accepted 14 March 2006; published 23 June 2006.

[1] The surface of Mars appears dramatically different between the northern and southern hemispheres. Any endogenic origin for this hemispheric dichotomy must involve a pattern of mantle convection that reflects the shape of the dichotomy, primarily spherical harmonic degree-1. We investigated two mechanisms by which degree-1 convection may be initiated in the Martian mantle: (1) an endothermic phase change near the CMB and (2) viscosity layering in the mid-mantle. Using two-dimensional (2-D) and 3-D spherical finite-element convection models, we explored the conditions under which each mechanism can produce degree-1 structures. The phase transition is only effective at generating degree-1 structures when the mantle viscosity is constant or weakly temperature-dependent (activation energy <100 kJ/mol), but the degree-1 pattern requires several billion years to develop. Increasing convective vigor in phase change models leads to reduced wavelengths for convective structures. Degree-1 convection can also develop in a layered viscosity mantle, with temperature- and depth-dependent viscosity. An overall sublithospheric radial viscosity variation of a factor of 100 including a factor of 8–25 jump in the midmantle can lead to formation of degree-1 structure in a timescale ranging from 100 My to several hundred My, consistent with the timescale for the formation of the dichotomy. Neither convective vigor nor the internal heating rate greatly affects the formation of degree-1 structures. We propose that degree-1 mantle convection induced by a layered viscosity structure may be responsible for the formation of the crustal dichotomy.

**Citation:** Roberts, J. H., and S. Zhong (2006), Degree-1 convection in the Martian mantle and the origin of the hemispheric dichotomy, *J. Geophys. Res.*, *111*, E06013, doi:10.1029/2005JE002668.

### 1. Introduction

#### 1.1. Origin of Crustal Dichotomy

[2] The hemispheric dichotomy is the most prominent topographic feature on Mars. This feature is largely an expression of thicker crust in the southern hemisphere [Hartmann, 1973; Zuber *et al.*, 2000] and hence is often called the crustal dichotomy. Formation of the crustal dichotomy, as one of the most important geological events, is likely to have significant effects on thermal evolution history of Mars and formation of other geological features including the Tharsis rise [Nimmo and Tanaka, 2005; Solomon *et al.*, 2005]. Therefore understanding the origin of crustal dichotomy is important in Martian science.

[3] MOLA gravity and topography data constrain the average crustal thickness to be 45 km, and 32 km and 58 km for northern lowlands and southern highlands, respectively [Zuber *et al.*, 2000; Neumann *et al.*, 2004; Wieczorek and Zuber, 2004]. Geochemical studies on

limited number of Martian meteorites suggest that significant amount of crustal materials may form shortly after initial differentiation of Mars [Halliday *et al.*, 2001] and possibly as a result of solidification of a magma ocean [Elkins-Tanton *et al.*, 2003]. Although significant progress has been made recently regarding the nature of the crustal dichotomy, its origin remains poorly understood.

[4] First, although it is generally accepted that crustal dichotomy is one of oldest features on Mars, disagreement for the timing of the dichotomy formation is significant enough to have implications for the formation mechanisms. Early studies on faulting and other tectonic features at the crustal dichotomy boundaries suggested a Late Noachian/Early Hesperian (3.7 Ga) formation for the dichotomy [McGill and Dimitriou, 1990]. However, most recent studies, motivated by the discovery of quasi-circular depressions (QCDs) in the northern lowlands [Frey *et al.*, 2002], suggest an Early Noachian or earlier (>3.93 Ga) formation time for the dichotomy. The QCDs are generally interpreted as buried impact craters and are suggestive that the basement of northern lowlands formed during the Early Noachian and is even older than visible highlands but perhaps slightly younger than the basement of southern highlands. This led Frey *et al.* [2002] and Nimmo and Tanaka [2005] to suggest that the dichotomy may have formed during or before the Early Noachian. Solomon *et al.* [2005] suggested that the

<sup>1</sup>Department of Astrophysical and Planetary Sciences, University of Colorado, Boulder, Colorado, USA.

<sup>2</sup>Department of Physics, University of Colorado, Boulder, Colorado, USA.

dichotomy formed at the same time as the bulk of the crust was created, i.e., 4.5 Ga.

[5] The second unresolved question is the formation mechanism for the crustal dichotomy. Proposed mechanisms include either exogenic process in the form of one or more giant impacts [Wilhelms and Squyres, 1984; Frey and Schultz, 1988] or endogenic processes including degree-1 mantle convection [Wise *et al.*, 1979; McGill and Dimitriou, 1990; Zhong and Zuber, 2001], plate tectonics [Sleep, 1994; Lenardic *et al.*, 2004], and mantle overturn following solidification of a magma ocean [Elkins-Tanton *et al.*, 2003]. While the viability of giant impact process remains an open question [Nimmo and Tanaka, 2005], this study focuses on endogenic processes, particularly degree-1 mantle convection.

[6] Degree-1 mantle convection is a particular convective structure in which one hemisphere is dominated by an upwelling, while the other hemisphere is mainly a downwelling. Zhong and Zuber [2001] showed that degree-1 mantle convection can be generated in a mantle with radial viscosity contrast of a factor of 500. Zhong and Zuber [2001] suggested that an upwelling in what is now the northern hemisphere may erode the overlying crust and accrete that crustal material onto the crust in the southern hemisphere, or that alternatively excess heat from a upwelling plume below the southern hemisphere may lead to a greater degree of melting and therefore a thicker crust above the plume in the southern hemisphere.

[7] Plate tectonics were originally proposed to explain the relatively thin crust in the northern lowlands with smooth and young (e.g., Hesperian) surface [Sleep, 1994]. However, the Early Noachian age for the basement of the northern lowlands [Frey *et al.*, 2002] suggests that plate tectonics must have operated before the Early Noachian if it operated at all. The plate tectonics hypothesis did not address why plate tectonics only operated in one hemisphere and therefore the origin of crustal dichotomy [Zhong and Zuber, 2001]. The hypothesis of mantle overturn following solidification of an early magma ocean that leads to crustal dichotomy [Elkins-Tanton *et al.*, 2003, 2005] is similar to a model proposed originally for lunar mare basalts [Parmentier *et al.*, 2002]. Following the extraction of crustal materials, the residue materials of the magma ocean may be denser than the underlying mantle. Depending on the thickness and viscosity of the residue materials, they may drive a Rayleigh-Taylor instability and mantle overturn at various wavelengths and timescales [Parmentier *et al.*, 2002] that may be related to the crustal dichotomy [Elkins-Tanton *et al.*, 2003, 2005].

[8] To assess the validity of each of these hypotheses is important but also difficult at this stage. This is mainly because for each hypothesis, the conditions for which the crustal dichotomy can be generated and its consequences for various observables are not well understood, and also partly because of significant uncertainties with currently available observations and their interpretations regarding the crustal dichotomy. Solomon *et al.* [2005] suggested that on the basis of their estimated timing of 4.5 Ga for dichotomy formation and the time required for mantle convection to produce a degree-1 structure, degree-1 mantle convection and plate tectonic processes are untenable. However, such an assessment depends on a number of assumptions that

have not been fully investigated. First, the dichotomy may have formed during the Early Noachian at  $\approx 4.0$  Ga [Frey *et al.*, 2002; Nimmo and Tanaka, 2005], which is  $\approx 500$  Ma after the timing suggested by Solomon *et al.* [2005]. Second, the time required by mantle convection to produce a degree-1 structure may strongly depend on mantle viscosity which is not well constrained. This dependence of timescales on mantle viscosity may not be that different from that for the mantle overturn of magma ocean residue. Moreover, geochemical studies suggest that the primordial crust that formed soon after the primary differentiation contains at least one-third of the present crustal volume [Norman, 1999; Wieczorek and Zuber, 2004], suggesting that some or all of the remaining crust may have been formed later, allowing a later formation time for the dichotomy than that suggested by Solomon *et al.* [2005].

[9] Therefore we believe that while more data and observations are needed, it is also important to understand the physics of each proposed model. The goal of this study is to examine the conditions under which degree-1 mantle convection can operate and the time-scales during which degree-1 mantle convection can be produced.

## 1.2. Mechanisms for Degree-1 Mantle Convection

[10] Several different mechanisms have been proposed to generate long-wavelength mantle convection. One is an endothermic spinel-perovskite phase transition. Phase changes have been shown to promote long-wavelengths in the Earth's mantle [Tackley *et al.*, 1993]. Depending on the mantle model, the spinel-perovskite phase change may exist just above the Martian core-mantle boundary (CMB) [Harder and Christensen, 1996; Breuer *et al.*, 1997; Harder, 2000]. This deep transition acts a barrier to convection, allowing only the longest wavelengths to penetrate it. Previous studies [Harder and Christensen, 1996; Harder, 2000] have demonstrated that a degree-1 convection pattern emerges when this transition is included. However, these studies only considered an isoviscous mantle beneath a high-viscosity lithosphere. Furthermore, Harder [2000] used an approximation for the heating, neglecting the frictional heating altogether and ignoring lateral variations in adiabatic and latent heating. While these studies were primarily motivated by finding a formation mechanism for Tharsis, not the dichotomy, the physical principles are the same for both features.

[11] A second method of producing a degree-1 structure is to consider a stratified mantle viscosity with a weak aesthenosphere. Earlier studies have shown that viscosity layering can lead to long wavelength structures in the Earth's mantle [Zhang and Yuen, 1995; Bunge *et al.*, 1996]. Zhong and Zuber [2001] showed that a sharp contrast in viscosity between the upper mantle and lower mantle of Mars may produce a degree-1 structure, given a sufficiently strong viscosity contrast. They modeled convection in a 2-D spherical axisymmetric geometry, and found that a temperature- and pressure-dependent viscosity mantle overlain by a high-viscosity lid is dominated by small plume structures. When they reduced the strength of the upper mantle by a factor of 500, a degree-1 pattern developed. Such a step change in viscosity may be attributed to a number of mechanisms, including compositional variation associated with the residue from an early magma

**Table 1.** Model Parameters: Phase Changes

Parameter	Value
Planetary radius	3400 km
Core radius	1450 km
Lithospheric thickness	220 km
Gravitational acceleration	$3.5 \text{ m s}^{-2}$
Mantle density	$3500 \text{ kg m}^{-3}$
Thermal diffusivity	$10^{-6} \text{ m}^2 \text{ s}^{-1}$
Thermal expansivity at CMB	$2 \times 10^{-5} \text{ K}^{-1}$
Thermal expansivity at surface	$4 \times 10^{-5} \text{ K}^{-1}$
Specific heat	$1200 \text{ J K}^{-1} \text{ kg}^{-1}$
Temperature difference	2100 K
Surface temperature	500 K
Viscosity cutoff	$10^5$
Internal heating	$5.25 \times 10^{-9} \text{ W m}^{-3}$
Phase transitions	
Exothermic	
Radial position	2300 km
Clapeyron slope	$3 \times 10^9 \text{ Pa K}^{-1}$
Density change	$210 \text{ kg m}^{-3}$
Half-width	50 km
Endothermic	
Radial position	1520 km
Clapeyron slope	$-3 \times 10^6 \text{ Pa K}^{-1}$
Density change	$210 \text{ kg m}^{-3}$
Half-width	40 km

ocean, a transition from diffusion creep to dislocation creep, or from a phase transition. However, *Zhong and Zuber* [2001] considered a low value for activation volume relative to what the Earth's mantle is expected to have [*Karato and Jung*, 2003]. Furthermore, it is unclear whether 2-D axial symmetry may affect the formation of degree-1 structures.

[12] In this study, we have investigated these two mechanisms for producing degree-1: phase changes and viscosity layering. We have built on some of the past models and address some weaknesses of each one. For the phase change models, we expanded on the work of *Harder* [2000] and address three issues not considered in past studies on this topic. First, we considered the effect of temperature-dependent viscosity on the planform of convection in models with phase changes. Second, we used the complete heating formulation [*Christensen and Yuen*, 1985]. While we do not expect the heating to have a dramatic effect on the dynamics, we have included it for completeness. Third, we examined the timescale required to form degree-1 structures. *Harder and Christensen's* [1996] and *Harder's* [2000] models took a long time (several Gy) to develop degree-1 convection. Since they were primarily interested in forming Tharsis, which was considered at the time to be a much younger feature than the crustal dichotomy [*Tanaka et al.*, 1992], these models were therefore not so concerned about the timescale.

[13] The layered viscosity models build on the work of *Zhong and Zuber* [2001]. We address several key issues not covered in that work. First, we generalized the models to a 3-D geometry to examine if the same patterns seen in 2-D would hold up in 3-D. Second, we used a more realistic rheology. In addition to the viscosity jump we considered much stronger temperature- and pressure-dependence [*Karato and Jung*, 2003], which increased the continuous viscosity variation with depth. Third, we examined the extent to which internal heating controls the wavelength

of the convection. *McNamara and Zhong* [2005] showed that a strongly internally heated mantle is more likely to produce long wavelengths than a basally heated mantle for mobile-lid convection. We experimented with a range of internal heating rates, consistent with either a primordial or a depleted mantle. Fourth, we examined the required magnitude of the viscosity jump and the total viscosity variation across the mantle. We explored a range in the magnitude of the viscosity jump and the continuous pressure dependence of viscosity. Finally, we also examined the timescale required to form a degree-1 structure in a layered viscosity mantle.

[14] In this paper, we first present a description of the governing equations and the computational tools used to create our convection models. In section 3, we present the results of our modeling, both with phase changes and with viscosity layering. We discuss the physical meaning of our results, and consider the feasibility of each mechanism for generating degree-1 convection in section 4. Finally, we present our conclusions.

## 2. Model Descriptions

[15] We consider the mantle to be an infinite Prandtl number fluid in a 3-D spherical shell. The mantle is both basally and internally heated. Convection can be described by the equations of conservation of mass, momentum and energy, assuming incompressibility and the extended Boussinesq approximation [*Christensen and Yuen*, 1985]. The nondimensionalized governing equations are

$$\nabla \cdot \vec{u} = 0, \quad (1)$$

$$-\nabla P + \nabla \cdot [\eta(\nabla \vec{u} + \nabla^T \vec{u})] + Ra\alpha(r)T\vec{e}_r - Rb_{o-s}\Gamma_{o-s}\vec{e}_r - Rb_{s-p}\Gamma_{s-p}\vec{e}_r = 0, \quad (2)$$

$$\frac{\partial T}{\partial t} + \vec{u} \cdot \nabla T = \kappa(r)\nabla^2 T + H_{int} + H_A + H_V + H_L, \quad (3)$$

where  $\vec{u}$  is the velocity,  $P$  is the pressure,  $\eta$  is the viscosity,  $T$  is the temperature, and  $\vec{e}_r$  is a unit vector in the radial direction.  $\alpha(r)$  and  $\kappa(r)$  are the depth-dependent thermal expansivity and thermal diffusivity, and vary linearly with radius. The thermal Rayleigh number,  $Ra$  is defined as

$$Ra = \frac{\rho_0 g \alpha_0 \Delta T R_0^3}{\kappa_0 \eta_0}, \quad (4)$$

where  $\rho_0$ ,  $\alpha_0$ ,  $\kappa_0$ , and  $\eta_0$  are the reference values for density, thermal expansivity, thermal diffusivity, and viscosity. We have chosen all reference values to be those at the bottom of the mantle. We allow both  $\alpha$  and  $\kappa$  to vary linearly with depth. Here  $g$  is the gravitational acceleration, and  $\Delta T$  is the temperature difference across the mantle.  $R_0$  is the radius of the planet. Note that we use this characteristic length scale in all nondimensionalizations, rather than the thickness of the convecting mantle  $d$ . Our Rayleigh numbers will therefore be higher than those in comparable convection

**Table 2.** Model Parameters: Layered Viscosity

Parameter	Value
Planetary radius	3400 km
Core radius	1650 km
Depth of layering	1020 km
Gravitational acceleration	3.73 m s <sup>-2</sup>
Mantle density	3400 kg m <sup>-3</sup>
Thermal diffusivity at CMB	2.132 × 10 <sup>-6</sup> m <sup>2</sup> s <sup>-1</sup>
Thermal diffusivity at surface	1.066 × 10 <sup>-6</sup> m <sup>2</sup> s <sup>-1</sup>
Thermal expansivity at CMB	2 × 10 <sup>-5</sup> K <sup>-1</sup>
Thermal expansivity at surface	4 × 10 <sup>-5</sup> K <sup>-1</sup>
Specific heat	1200 J K <sup>-1</sup> kg <sup>-1</sup>
Temperature difference	1980 K
Surface temperature	220 K
Activation energy	157 kJ mol <sup>-1</sup>
Default internal heating rate	7.4 × 10 <sup>-8</sup> W m <sup>-3</sup>

studies which normalize to  $d$ , by a factor of  $(R_0/d)^3$ . All these parameters are listed in Table 1 for the phase change calculations and Table 2 for the viscosity layering calculations.

[16] In equation (2),  $\Gamma_{o-s}$  is a phase function for the transition from olivine to spinel, while  $\Gamma_{s-p}$  is for the spinel to perovskite change [Christensen and Yuen, 1985]. The phase change Rayleigh number is

$$Rb = \frac{\delta\rho}{\rho_0\alpha_0\Delta T} Ra, \quad (5)$$

where  $\delta\rho$  is the density change associated with the phase change (Table 1).

[17] We include several heating terms in the energy equation (3).  $H_{int}$  is the rate of internal heat production,  $H_A$  and  $H_V$  represent the heating due to adiabatic compression and viscous dissipation, respectively and  $H_L$  is the latent heat of the phase transitions [Christensen and Yuen, 1985].

[18] The nondimensional internal heating rate is given by

$$H_{int} = \frac{QR_0^2}{\rho_0 C \Delta T \kappa_0}, \quad (6)$$

where  $Q$  is the internal heating rate measured as energy per time per volume, and  $C$  is the specific heat. Material crossing the phase transitions absorbs or releases latent heat according to the nondimensional equation

$$H_L = \gamma \frac{\alpha_0 T Rb}{\rho_0 C Ra}, \quad (7)$$

where  $\gamma$  is the Clapeyron slope.

[19] Although plate tectonic-style mantle convection has been suggested for early Mars [Sleep, 1994; Nimmo and Stevenson, 2001; Lenardic et al., 2004], in this study we only considered stagnant-lid convection which is realized through either depth-dependent or temperature-dependent viscosity. The nondimensional viscosity,  $\eta$ , is given by

$$\eta = \eta'(r) \exp\left[\frac{E' + V'(1-r)}{T + T_s} - \frac{E' + V'(1-r_{core})}{1 + T_s}\right], \quad (8)$$

using the following normalizations:

$$E' = \frac{E}{R\Delta T}, \quad V' = \frac{\rho_0 g R_0 V}{R\Delta T}, \quad T_s = \frac{T_{surf}}{\Delta T}, \quad (9)$$

where  $E$  is the activation energy,  $V$  is the activation volume,  $R$  is the gas constant,  $T_{surf}$  is the surface temperature,  $r$  is the nondimensional radial position, and  $r_{core}$  is the core radius. Here  $\eta'(r)$  is a radial viscosity profile (e.g., layering) upon which the temperature- and pressure-dependence is superimposed;  $\eta$  has been normalized to the viscosity at the CMB.

[20] For the calculations with phase changes, we were primarily concerned with the effect of temperature-dependent viscosity that was not considered by Harder [2000]. To better compare our results to those of Harder [2000], we neglected pressure-dependent viscosity, and the viscosity formulation (8) reduces to

$$\eta = \eta'(r) \exp\left[\frac{E'}{T + T_s} - \frac{E'}{1 + T_s}\right], \quad (10)$$

where  $\eta'(r)$  in these cases describes a two-layer mantle: a high-viscosity lithospheric lid and a weaker interior. Following Harder [2000], the thermal diffusivity was held constant. The parameters for these calculations are given in Table 1.

[21] For the models with viscosity layering, the phase transitions were not included in order to isolate the effect of viscosity layering. Equations (2) and (3) reduce to

$$-\nabla P + \nabla \cdot [\eta(\nabla \vec{u} + \nabla^T \vec{u})] + Ra\alpha(r)T\vec{e}_r = 0 \quad (11)$$

$$\frac{\partial T}{\partial t} + \vec{u} \cdot \nabla T = \kappa(r)\nabla^2 T + H_{int} + H_A + H_V. \quad (12)$$

[22] Again,  $\eta'(r)$  describes two viscosity layers. To represent the sharp viscosity change with depth in the mid-mantle, a step function in viscosity was imposed at that depth [Zhong and Zuber, 2001]. Rather than using a third layer to impose a lithosphere, we allowed this high-viscosity lid to develop out of the temperature-dependence. See Table 2 for the parameters used in the layered viscosity calculations. Note that these parameters were chosen to be consistent with those of Zhong and Zuber [2001]. Although a few of the values are somewhat different from those used in the phase change models, the results are not sensitive to the choice of parameters.

[23] For all calculations, isothermal and free-slip boundary conditions were imposed at the surface and the CMB. For each case, we first used a finite-element convection code modified from Citcom [Zhong, 2002; Roberts and Zhong, 2004] to solve these governing equations (1)–(3) in a 2-D axisymmetric spherical geometry on a grid of 64 elements in radius and 256 elements in latitude. We ran each calculation until the system heat flow reached a steady state. We then used CitcomS [Zhong et al., 2000] to perform each calculation in a 3-D spherical geometry using the final horizontally-averaged temperature profile from the corresponding 2-D case as the initial temperature condi-

**Table 3.** Parameters for Phase Change Calculations

Case	$Ra_{bottom}$	$Ra_{interior}$	E, kJ/mol	Final Time Step	Final Time, Gy
P1	$2 \times 10^7$	$2 \times 10^7$	0	56000	7.6
P2	$6 \times 10^7$	$1.29 \times 10^7$	50	49000	11.5
P3	$2 \times 10^8$	$2.02 \times 10^7$	100	42200	12.4
P4	$2 \times 10^8$	$2.02 \times 10^7$	0	36000	9.1
P5	$2 \times 10^8$	$2 \times 10^8$	0	65600	4.8
P6	$6 \times 10^8$	$2.07 \times 10^8$	50	51300	3.4

tion. The 3-D shell was broken into twelve caps, each of which contained a grid of 48 elements in each horizontal direction, and either 48 or 64 elements in the radial direction. The calculations were done on a PC-cluster with either 12 or 24 Xeon processors. We ran these calculations until the convective planform became stable and no further evolution was likely.

### 3. Results

[24] Here we give the results of the convection models involving phase transitions and viscosity layering. We present a total of six calculations for the phase change models, and thirteen for the viscosity layering.

#### 3.1. Phase Transitions

[25] The first set of calculations test the model devised by *Harder* [2000] of using phase transitions as a mechanism of producing degree-1 (or one-plume) mantle convection for Mars. We ran several calculations which included both the endothermic spinel-perovskite transition and the exothermic olivine-spinel transition (also included in the work of *Harder* [2000]). We used parameters (Table 1) similar to those of *Harder* [2000], except that we have used the full version of the heating terms [*Christensen and Yuen*, 1985]. *Harder* [2000] did not consider lateral variations in the adiabatic and latent heating and omitted the frictional heating. To examine the role of temperature-dependent viscosity, we used several different values of activation energy. Parameters specific to each individual case are detailed in Table 3. Following *Harder* [2000], a degree-4 perturbation was applied to the initial temperature field. This same perturbation was applied to all subsequent phase change calculations.

[26] The first goal was to reproduce the model result of *Harder* [2000] with a single plume structure. Case P1 has an isoviscous mantle, capped by a 220-km-thick lithosphere with viscosity  $10^5$  times that of the mantle. This case was run using the same parameters used by *Harder* [2000], and the only difference is the treatment of heating terms, as described earlier. Early in the calculation, the perturbed harmonic,  $\ell = 4$  quickly becomes dominant. However, similar to what *Harder* had demonstrated, the  $\ell = 1$  component grew and a single plume structure arose after nearly 5 Gy (Figure 1a). To examine the effect of the initial condition on the final planform, we repeated the case with a random initial perturbation. No significant changes were observed and degree-1 became the dominant structure.

[27] *Harder's* [2000] model and our case P1 assume that the sublithospheric mantle has a constant viscosity. Mantle

viscosity depends on temperature, however. To test the extent to which this temperature-dependence affects the convective planform, two more calculations were performed in which relatively low activation energies were used. Cases P2 and P3 have  $E = 50$  and  $100$  kJ/mol, respectively (Table 3). Because the viscosity is referenced to that at the bottom of the mantle, temperature dependence increases the mantle viscosity significantly. Therefore we have increased  $Ra$  in cases P2 and P3 (Table 3) in order to keep the average mantle viscosity comparable to case P1 (Figures 1d and 1e).

[28] Similar to case P1, case P2 with  $E = 50$  kJ/mol, produced a single plume (Figure 1b), but this pattern took much longer to develop than in case P1, about 9 Gy. However, case P3, with  $E = 100$  kJ/mol was dominated by much smaller wavelengths ( $\ell = 10$ ) than the previous cases, despite the use of the same initial perturbation. The power stayed at this wavelength for the duration of the calculation. About 30 plumes survived even after more than 12 Gy (Figure 1c).

[29] The latent heat from the phase changes affects the radial temperature profiles of the models. Material changing from olivine to spinel releases heat and increases the mantle temperature beneath the phase transition. This effect is evident as a kink in the radial temperature profiles at about 1000 km depth (Figure 1d). Likewise, material descending through the spinel-perovskite transition absorbs heat and should cause a kink in the opposite direction [*Turcotte and Schubert*, 2002]. However, this endothermic phase transition is so close to the CMB in these models that it is within the thermal boundary layer, at about 1880 km depth. For cases P1 and P2, the kink cannot be seen in the radial profile. A kink can be seen for case P3, but of a greater magnitude than would be expected from the latent heat alone. Case P3 has a weaker lower mantle due to stronger temperature-dependent viscosity (Figure 1e). The radial velocity for case P3 drops off at the depth of the phase transition (Figure 1f), suggesting that it is undergoing two-layer convection. This layered convection, is probably responsible for the kink seen in the radial temperature profile for case P3, rather than the latent heat effect.

[30] *Tackley* [1996] suggested on the basis of models with no phase changes that the radial viscosity structure controls the flow pattern and that lateral variations in viscosity are not important to the general planform of convection. This prompted us to examine the possibility that radial viscosity in case P3 with  $E = 100$  KJ/mol (Figure 1e) is responsible for the short wavelength structure. At a first glance, this seems to be consistent with the much reduced viscosity in the bottom thermal boundary layer for case P3 (Figure 1d), which may enhance small scale instability. To test this idea, case P4 used the horizontally averaged viscosity from case P3 as the radial viscosity, but excluded the temperature-dependent viscosity. Although many plumes developed early, the power steadily shifted to lower harmonics. A single degree-1 plume formed after 9 Gy (Figure 2). The difference between these results and the fully temperature-dependent calculation (i.e., case P3) suggests that lateral variation in viscosity may play an important role here in affecting planform of convection and producing short wavelength structures, given the radial viscosity variations used here.

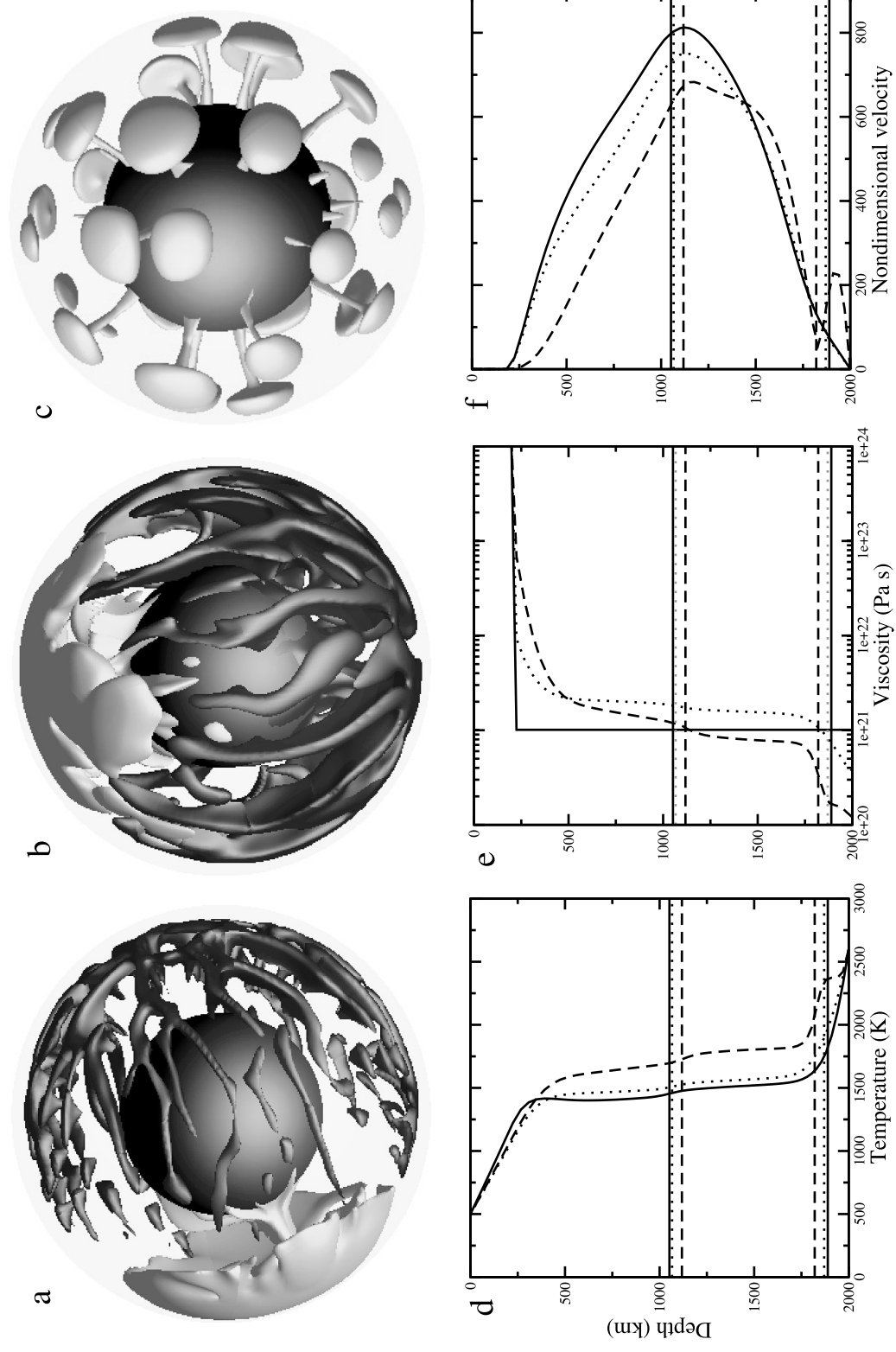


**Figure 1.** Residual temperature of convection calculations with phase changes. Upwellings are light-colored, downwellings are dark. The isosurfaces represent upwellings (downwellings) in which the nondimensional temperature is greater (lower) the mean temperature at that depth by an amount specific to each case. Shown are the isosurfaces for (a) case P1 at 7.6 Gy with residual temperature = +0.05 (-0.03), (b) case P2 at 11.6 Gy with residual temperature = ±0.05, and (c) case P3 at 7.7 Gy with residual temperature = +0.05. For clarity, downwellings have been omitted from figure 1c. (d) Depth-dependent temperature, (e) viscosity, and (f) radial velocity profiles for cases P1–P3. P1, solid line; P2, dotted line; P3, dashed line. Mean positions of the phase transitions are shown as horizontal lines on Figures 1d–1f in the same line style as the associated case. Phase transition depth is temperature dependent. Evolution of the temperature structure has caused the transitions to shift.

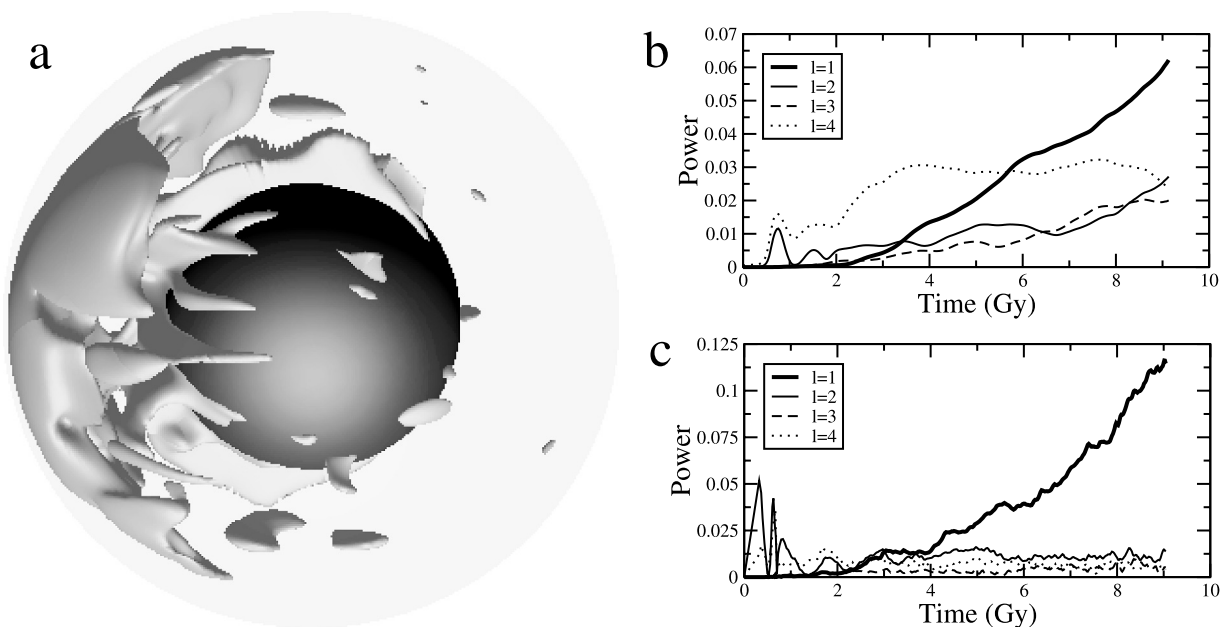


**Figure 2.** Convection model considering only radial variation in viscosity (Case P4). Radial viscosity profile equivalent to that when  $E = 100$  kJ/mol, but this case excluded actual temperature-dependent viscosity. (a) Upwellings with isosurface of 0.03 above background temperature at time = 9.1 Gy. Time-dependent spectrum of convective structures at the first four harmonics at (b) 220 km depth and (c) 1880 km depth.

[31] These results suggest that phase transitions can promote degree-1 convective patterns, but only if the mantle viscosity is constant or weakly temperature dependent. However, the timescales required to develop these structures (several Gy) are inconsistent with the formation of the crustal dichotomy (500 My). Since the timing is dependent on flow velocity and therefore on convective vigor, we tested whether an increase in  $Ra$  might generate degree-1 structures more quickly.  $Ra$  from our degree-1 cases (P1 and P2) was increased by a factor of 10 and the calculations were redone (cases P5 and P6 in Table 3). However, the stronger convection promoted more instabilities of short wavelengths rather than a swifter onset of degree-1 convection, as demonstrated by multiple plumes (Figures 3a and 3b). There is virtually no power at degree-1 and the system is dominated by much higher harmonics ( $\ell = 6-10$ ). The power remains at these short wavelengths throughout the calculation (Figures 3c–3f) and suggests that growth of degree-1 is highly unlikely.

### 3.2. Viscosity Layering

[32] The results presented here expand on the model of *Zhong and Zuber* [2001], using a layered viscosity structure to help produce degree-1 convection in the Martian mantle. We ran a total of 13 calculations for this model, testing the effects on the planform of convection of the magnitude of the viscosity jump, the internal heating rate, the convective vigor, and the total sublithospheric viscosity contrast. The input parameters for each case are shown in Table 4. The initial temperature field of each case was perturbed either randomly or with a short-wavelength harmonic ( $\ell = 51$ ). The final planform, however, is not sensitive to the choice of this initial condition.

[33] We first examined whether a viscosity jump such as that used by *Zhong and Zuber* [2001] was necessary to produce degree-1 structures, or if simply having a large continuous viscosity variation across the mantle was sufficient. If the latter were true, then a continuous variation should produce a degree-1 pattern as easily as a localized viscosity jump of the same magnitude. Our first calculation, case V1, has a strongly temperature- and pressure-dependent viscosity, but no jump. Cases V2 and V3 have viscosity jumps of a factor of 8 and 25 respectively at a depth of 1000 km. An increase in viscosity of about this magnitude is suggested for the Earth at a similar pressure on the basis of long-wavelength geoid models [*Hager and Richards*, 1989], so its inclusion in this study is justified. The depth of the viscosity jump in our calculations roughly corresponds to the depth of the olivine-spinel phase transition, although the phase change dynamics were not included. The activation volumes in Cases V2 and V3 have been reduced in order to maintain a similar overall viscosity variation across the sublithospheric mantle. Thus we may identify the effect of the viscosity jump alone. Figure 4 shows the radial viscosity profiles for these three cases. This viscosity variation, of about a factor of 100 is consistent with the experiments of *Karato and Wu* [1993] and the rheology assumed for terrestrial studies [*Hager and Richards*, 1989; *King and Masters*, 1992; *Bunge et al.*, 1996].

[34] The final flow pattern for case V1 consists of two nearly antipodal plumes (Figure 5a). Case V2 also develops a two-plume structure. After a sufficiently long time, the two plumes connect and form a ridge. The stronger plumes can still be seen at the endpoints of the ridge in Figure 5b. Case V3 quickly develops a single upwelling (Figure 5c).

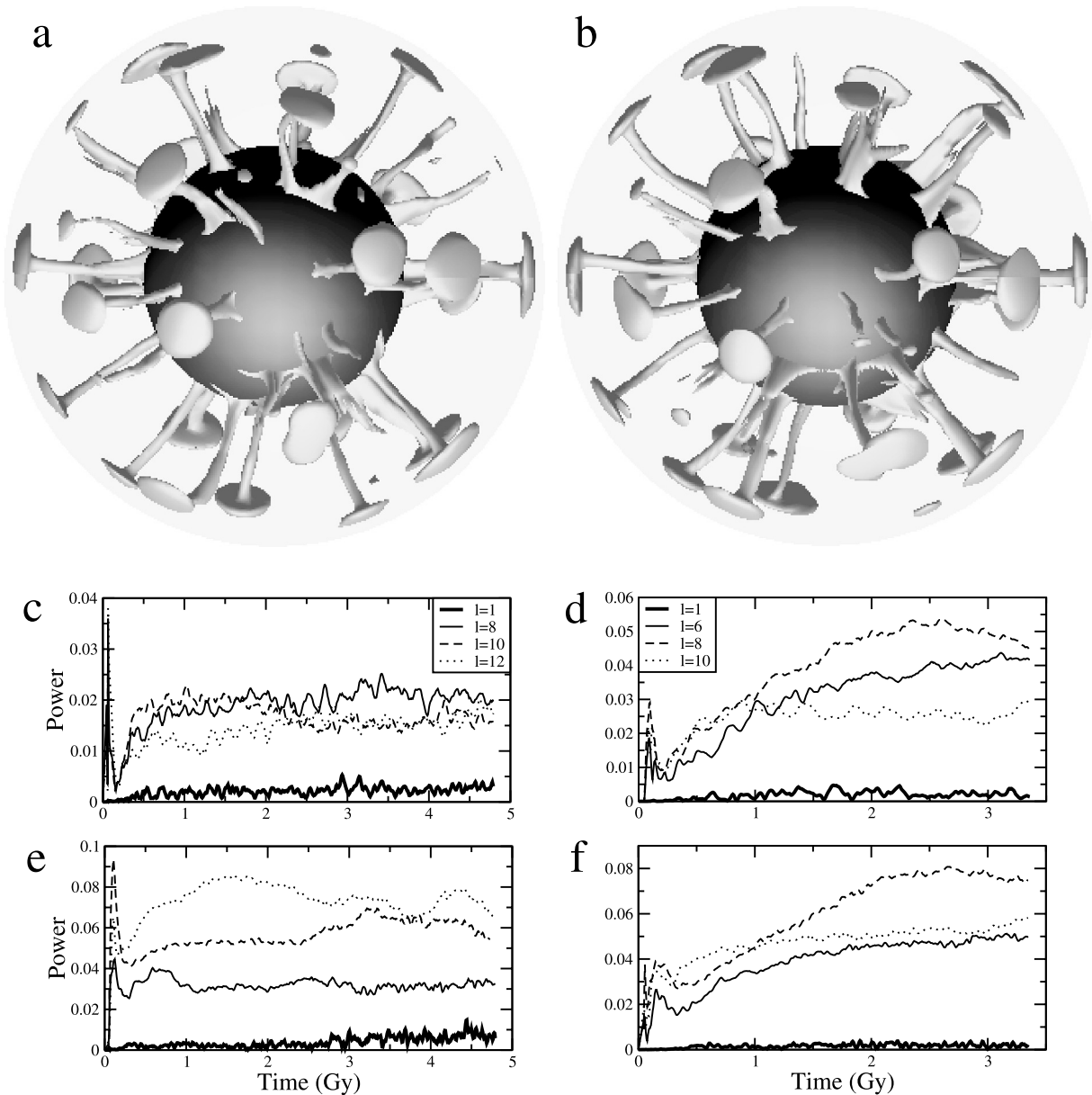


**Figure 3.** Convection calculations with phase changes using high  $Ra$  ( $2 \times 10^8$ ). Upwellings in (a) case P5 with isoviscous interior and (b) case P6 ( $E = 50\text{kJ/mol}$ ). The time in both cases is 3 Gy and the isosurfaces represent temperature 0.03 above background. Spectrum of convective structures for case P5 at (c) 270 km depth and (e) 1880 km depth, and for case P6 at (d) 270 km depth and (f) 1880 km depth.

[35] The evolution of the power at the longest wavelengths is shown in Figures 5d–5i for cases V1–V3. Degree-1 became the dominant spherical harmonic by 410 My and 175 My after the start of the calculation for cases V2 and V3, respectively. The time to reach  $\ell = 1$  (as reported in Table 4) is determined as the time when  $\ell = 1$  is the degree with the most power near the surface (110 km depth) and near the CMB (1670 km depth). This is the time after which degree-1 controls the convection, although in some cases, the power at degree-1 continues to increase and the appearance of the upwelling continues to improve for some time after this. The timescales for cases V2 and V3 are consistent with a rapid formation of

the crustal dichotomy [Frey *et al.*, 2002]. Comparison between cases V1–V3 suggests that a rapid change in radial viscosity is important for producing degree-1 structure, even when the total viscosity contrast is held approximately the same. Case V1 has no discontinuous viscosity variation and never approached degree-1. Rather, the two-plume structure seen in this case is predominantly  $\ell = 2$ , as evidenced by the power spectrum of temperature structures (Figures 5d and 5g). Case V2 has a two-plume structure in its early stage, but develops into a single upwelling, though that structure is more of a linear ridge than a classical plume. While  $\ell = 2$  dominates early on,  $\ell = 1$  eventually takes over (Figures 5e and 5h). Case V3 has significantly less power at shorter wavelengths

Table 4. Parameters for Layered Viscosity Cases<sup>a</sup>

Case	$\eta$		$V$ , $\text{cm}^3$ mol	$Q$ (Q0) <sup>b</sup>	$R_{\text{bottom}}$	Perturb.	Final Time		$\eta_{\text{min}}$	$Ra_{\text{int}}$ ( $10^9$ )	$T_{\text{int}}^c$	$v_{r,\text{max}}^c$	$Q_s^c$	$f_{\text{lims}}$ , %	Time to $\ell = 1$ , My	Number of Plumes		
	$\eta_{\text{lower}}$	$\eta_{\text{upper}}$					Steps	My								2-D	3-D	
V1	1	1	5.69	1.0	$1.25 \times 10^8$	random	46500	673	138	1.917	0.780	3532	35.2	83	never	ring	2	
V2	8	1	3.61	1.0	$1.25 \times 10^8$	random	60800	687	107	2.54	0.787	4533	34.1	83	410	2	ridge	
V3	25	1	2.69	1.0	$1.25 \times 10^8$	random	50200	447	119	2.65	0.789	5936	38.3	85	175	1	1	
V3a <sup>d</sup>	25	1	2.69	1.0	$1.25 \times 10^8$	random	42600	243	115	4.41	0.829	7577	42.6	89	163	1	1	
V3b <sup>d</sup>	25	1	2.69	1.0	$1.25 \times 10^8$	random	50100	214	116	5.52	0.849	7470	40.7	89	113	1	1	
V4	8	0.5	3.61	0.5	$8.6 \times 10^8$	$\ell, m = 51$	48600	324	161	3.39	0.688	5425	34.1	69	201	2	ridge	
V5	25	0.5	2.69	0.5	$8.6 \times 10^8$	$\ell, m = 51$	43000	254	161	3.43	0.675	6034	31.7	66	125	3	ridge	
V6	25	0.25	2.69	0.25	$4.5 \times 10^9$	$\ell, m = 51$	71700	315	218	4.09	0.593	6770	28.1	46	138	1	10 <sup>e</sup>	
V7	25	1.0	2.69	1.0	$1.00 \times 10^9$	$\ell, m = 51, 0^f$	41900	165	146	7.39	0.715	12510	47.1	76	98	2	1	
V8	1	1.0	8.00	1.0	$6.25 \times 10^6$	random	40000	943	857	1.121	0.795	1942	31.4	92	never	ring	1	
V9	8	1.0	6.30	1.0	$6.25 \times 10^6$	random	41600	1134	1308	1.331	0.780	2380	31.1	91	149	1	ridge	
V10	25	1.0	5.38	1.0	$6.25 \times 10^6$	random	58000	1361	1510	1.443	0.766	2494	31.2	90	87	1	ridge	
V11	8	0.5	6.30	0.5	$2.50 \times 10^7$	random	61800	1564	1720	0.865	0.675	1421	17.5	75	226	2	ridge	
V12	25	0.5	5.38	0.5	$2.50 \times 10^7$	random	42700	1119	1170	0.855	0.667	1789	18.9	77	176	1	ridge	
V13	25	1.0	5.38	1.0	$5.00 \times 10^7$	random	40000	369	2850	3.96	0.690	4408	36.6	84	146	2	ridge	

<sup>a</sup>Columns 2–6 show the input parameters for each case, columns 7–17 show the status at the end of the calculation.  $T$  may be dimensionalized by  $\Delta T$ ,  $v$  by  $\frac{K}{R_0}$ , and  $Q_s$  by  $\rho C_K \frac{\Delta T}{R_0}$ .  
<sup>b</sup>Internal Heating is given in terms of the default value in Table 2.

<sup>c</sup>Nondimensional values given for interior temperature (at 1000 km depth), maximum radial velocity, and surface heat flux.

<sup>d</sup>Cases V3a and V3b are identical to case V3 except that the resolution for each cap has been raised to  $64 \times 64 \times 96$  and  $96 \times 96 \times 64$  respectively. Note that these two cases have not been run for as long as case V3, and the final values should not be compared to case V3. The final time in case V3b is equivalent to that at time step 24000 in case V3, at which time  $Ra_{\text{int}} = 3.71 \times 10^9$ ,  $T_{\text{int}} = 0.815$ ,  $v_{r,\text{max}} = 7320$ ,  $Q_s = 44.0$ , and  $f_{\text{lim}} = 88\%$ .

<sup>e</sup>The plumes are all in the same hemisphere, very close to each other. The structure is largely  $\ell = 1$ .

<sup>f</sup>Case V7 was also run with a  $\ell, m = 51$  perturbation.

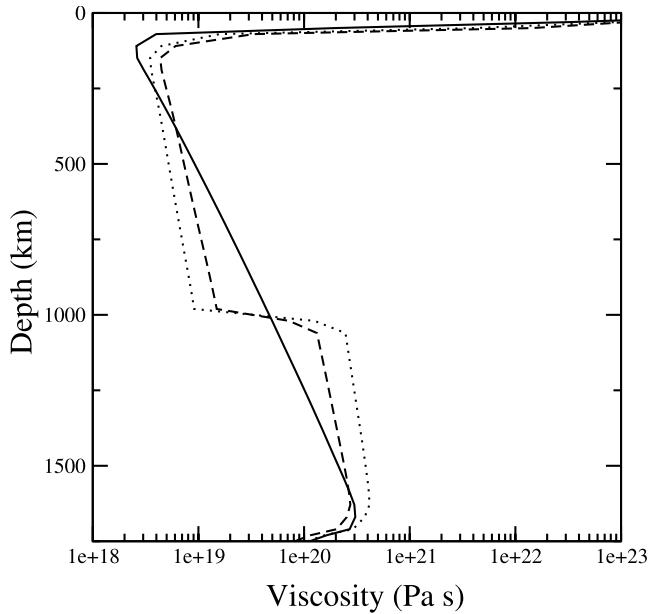


**Figure 4.** Viscosity profiles for cases V1 (solid line), V2 (dashed line), and V3 (dotted line).

than the other cases (Figures 5f and 5i). This progression demonstrates that the degree-1 becomes easier to produce as the size of the jump increases. However, even a relatively small jump as in case V2 is sufficient to generate a single upwelling and hemispheric asymmetry.

[36] While a one-plume structure as a final stable configuration is interesting, it is also worth examining the development of such a structure. Figure 6 illustrates the time evolution of case V3 into the single-plume structure. Initially a random perturbation is applied to the temperature field and a fairly short-wavelength structure develops early on (Figure 6a). The flow field quickly organizes itself into a ring structure in the lower mantle with a few plumes rising off of it (Figure 6b). Parts of the ring become stronger and other parts weaken, until eventually the ring breaks (Figure 6c). This remnant shrinks toward one hemisphere forming a ridge (Figure 6d). The ridge continues to shrink until it assumes a more classical plume shape (Figure 6e). This plume then persists for the duration of the calculation.

[37] We note that locally,  $Ra$  values of order  $10^9$  may be obtained. We therefore performed two additional calculations to demonstrate that small-scale features are not being artificially damped out by the resolution of our mesh. Cases V3a and V3b are identical to case V3, except that we have increased the resolution. Each cap in case V3a has 64 elements in each direction for case V3a, and 64 elements vertically and 96 elements in each horizontal direction for case V3b. This latter mesh corresponds to a factor of 5.3 increase in resolution over case V3. In all cases, a single plume develops and the degree-1 structure is maintained (Figure 6f). While the heat flow for these three cases behaves differently during the early stage of the calculations, the values converge after this period. After 200 My, the surface heat flow is 44.9, 43.4, and 40.9 for cases V3, V3a, and V3b, respectively. Because each case is started

with a random perturbation to the temperature field, the cases will have slightly different initial conditions. There may be some effect of this on the results. However, there is no significant effect on the development of the degree-1 structure.

[38] Heating mode may be another important control on the dominant wavelength of the final convective pattern. In a study of mobile-lid convection for the Earth, *McNamara and Zhong* [2005] found that models with purely temperature-dependent viscosity that are primarily heated from within tend to form much longer wavelengths than those that are basally heated. They did not consider pressure- or depth-dependent viscosity. We tested the effect of reduced internal heating on the convection in our stagnant-lid models. Cases V4 and V5 are identical to cases V2 and V3 except that the heating has been reduced by half (Table 4). Reducing the amount of heating results in a cooler mantle as shown in Figure 7a. Because a cooler mantle has a higher viscosity, we have increased  $Ra$  for these cases in order to maintain a similar viscosity structure as the high heating cases (Figure 7b).

[39] Both cases V4 and V5 develop a single degree-1 plume (Figures 8a and 8b) in 201 and 125 My, respectively, comparable to those from cases V2 and V3. The upwellings are more linear or ridge-like than those in the more strongly heated cases. To further test the effect of heating, we reduced the internal heat even further in case V6, giving it only one fourth the original heating rate. Degree-1 convection still develops after about 138 My, however, this is expressed as a “forest” of plumes in one hemisphere rather than a single upwelling (Figure 8c). A further 180 My of development does not change this pattern in any significant way. A significant fraction of basal heating ( $\sim 50\%$ ), changes the convective structure such that there are many upwellings rather than just one, even though the spectrum is still largely  $\ell = 1$ .

[40] While the required 175 My for case V3 to develop degree-1 convection may be sufficiently quick to predate the dichotomy [*Frey et al.*, 2002; *Nimmo and Tanaka*, 2005], arguments have been made for an even older dichotomy, within the first 100 My [*Solomon et al.*, 2005]. Because the actual timescale for degree-1 formation depends on the choice of  $Ra$ , increasing the convective vigor may speed up the degree-1 formation rate. Case V7 is the same as case V3, except that we have raised  $Ra$  by a factor of 8. Indeed, a single plume develops in this case as well (Figure 9a), and degree-1 becomes the strongest harmonic by 98 My (Figures 9b and 9c). Unlike in the phase change calculations, more vigorous convection leads to more rapid formation of a degree-1 pattern in a mantle with layered viscosity. Case V7 was also run with two different initial perturbations ( $\ell = 51, m = 0$ , and  $\ell = 51, m = 51$ ). We saw no significant differences between the results, including the time-dependence from these two trials and conclude that our choice of initial condition does not affect the final results.

[41] Cases V1–V7 have a total viscosity contrast of order 100 across the sublithospheric mantle. While this is consistent with the rheological parameters suggested by *Karato and Wu* [1993] (adjusted for diffusion creep) and with many terrestrial studies [*Hager and Richards*, 1989; *King and Masters*, 1992; *Bunge et al.*, 1996], recent experiments

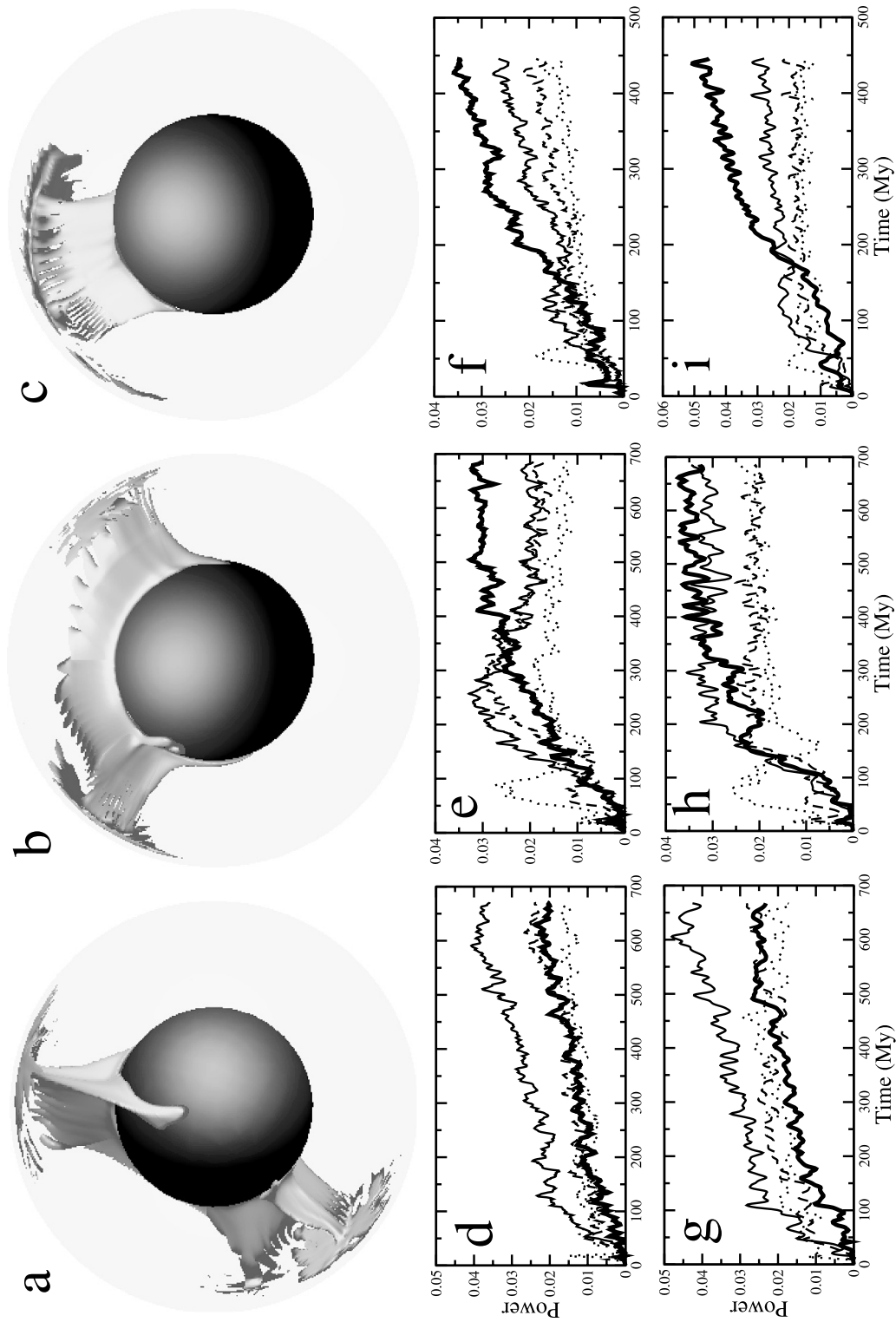


**Figure 5.** Isosurfaces represent upwellings with residual temperature  $\geq 0.04$  for (a) case V1 at 670 My, (b) case V2 at 450 My, and (c) case V3 at 250 My. Downwellings have been omitted for clarity. Time-dependent spectra of temperature structures at the first four spherical harmonics at a depth of 110 km for cases (d) V1, (e) V2, and (f) V3. Spectra at 1670 km depth for cases (g) V1, (h) V2, and (i) V3. Here  $\ell = 1-4$  are represented by thick solid, thin solid, dashed, and dotted lines, respectively.

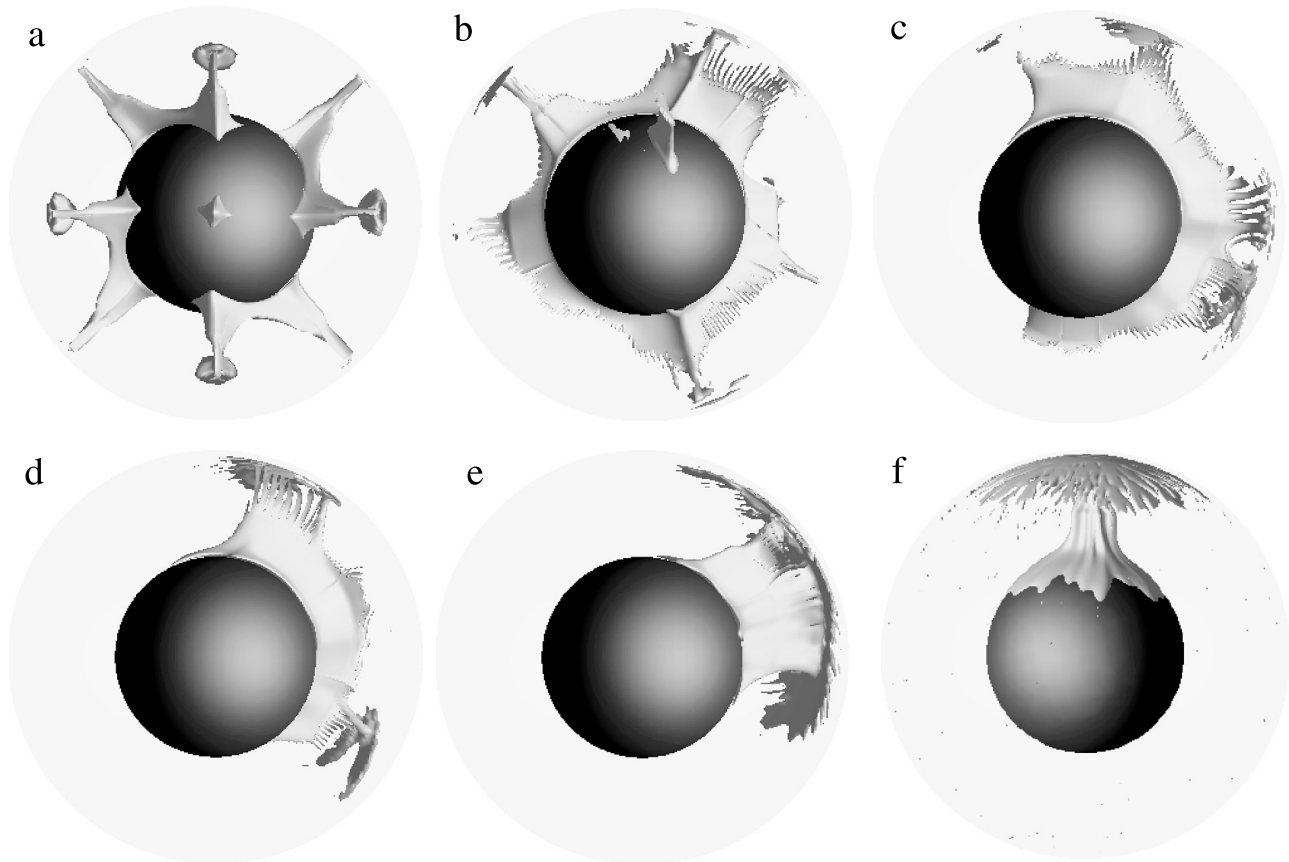


**Figure 6.** Evolution of upwelling structures in case V3. Isosurfaces show upwellings with residual temperature  $\geq 0.03$ . The downwellings have been omitted for clarity. (a) Time = 16 My: many short-wavelength structures. (b) Time = 90 My: ring forms in lower mantle with a few plumes rising off it. (c) Time = 160 My: ring weakens and breaks on one side. (d) Time = 190 My: ridge shrinks in extent, concentrates in one hemisphere. (e) Time = 250 My: ridge contracts to a plume. (f) Upwelling plume for case V3b with increased resolution at time = 214 My.

suggest a higher activation volume, resulting in a viscosity variation that is an order of magnitude larger [Karato and Jung, 2003]. To test the effect of this stronger pressure dependence, we ran another set of calculations using increased activation volume,  $V$ . Cases V8–V10 are identical to V1–V3, except that  $V$  has been raised so as to give a total sublithospheric viscosity variation of about 1000. We also reduced  $Ra$  for cases V8–V10 so that the effective Rayleigh number in those calculations is similar to that in cases V1–V3 (Table 4). Thus we may compare cases with similar vigor of convection.

[42] The final flow pattern for case V8, with no jump in viscosity, consists of a ring-shaped upwelling (Figure 10a). Like case V1, this pattern is dominated by  $\ell = 2$  (Figures 10b and 10c), but the expression is very different; a ring rather than two plumes. As before, no degree-1 convection ever develops without the presence of the viscosity jump.

[43] The inclusion of a viscosity jump did drive the system to degree-1. Case V9 developed a ring-like structure during the early stage of the calculations. However, after several tens of My the ring converged toward one hemisphere and folded up into a long linear ridge, rather than contracting into a more classical plume shape. Case V10

developed short wavelength upwellings early on, which then contracted into a plume and then spread out into a ridge. Figures 10d–10f show this progression for case V10. The resulting ridge is predominantly at degrees 1 (Figures 10g and 10h). The final state for case V9 looks very similar to case V10 except that the power at degree-2 is roughly equal to that at degree-1.

[44] The planforms of cases V8–V10 are somewhat different from cases V1–V3. Case V8 produces a degree-2 structure, but this is expressed as an upwelling ring, rather than as a pair of antipodal plumes as in case V1. Although the convection in cases V9 and V10 is largely degree-1, the large continuous viscosity contrast causes a single upwelling to spread out along one direction and form a ridge, rather than the plume such as that in case V3. In general, a higher total viscosity variation promotes more linear features and a low total viscosity variation promotes more axisymmetric plumes, regardless of the size of the discontinuous viscosity jump.

[45] We again experimented with lower heating values and increased convective vigor as we did for the lower  $V$  calculations (Table 4, cases V11–V13). We observed very similar behavior for these cases as we did for V4, V5, and

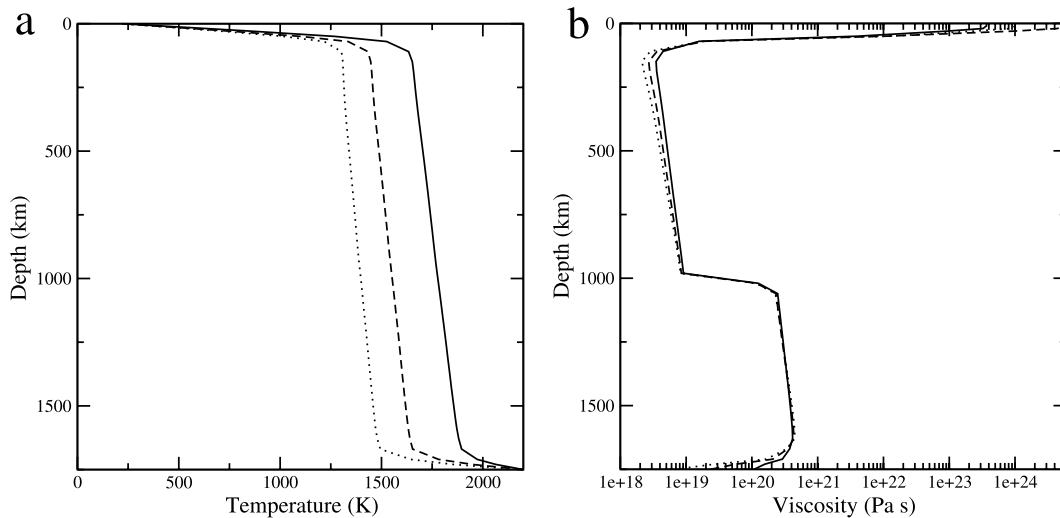


**Figure 7.** Radial (a) temperature and (b) viscosity profiles for cases with 25X viscosity jump and varying amounts of internal heating. Cases V3, V5, and V6 are represented by the solid, dashed, and dotted lines, respectively.

V7. Neither reducing the heating rate by half, nor increasing  $Ra$  by a factor of 8 has any significant effect on the development of degree-1 convection.

[46] Finally, we describe the effects of the geometry on the convective flow pattern. Because it is computationally much cheaper, it is tempting to run convection models in only two dimensions and assume axial symmetry. However, the 2-D axisymmetric approximation may produce false structures, considering that some 3-D structures have no 2-D analog. It is impossible to produce a ridge in 2-D, for example. In 2-D, an upwelling is interpreted as a plume at the pole, a ring near the equator and a cone at higher latitudes. In particular, one concern was that the poles may attract upwellings and downwellings, making degree-1 convection artificially easy to produce. Table 4 shows the final pattern for each case in both the 2-D and 3-D geometry. Although in most cases there is agreement between the two geometries, a single upwelling structure (i.e., degree-1 convection) arises more frequently in the 3-D

cases than in the 2-D cases. The additional flow patterns available in three dimensions make it easier, rather than harder to develop structures at  $\ell = 1$ . This suggests that 2-D axisymmetric models may often require more restrictive conditions than necessary to produce degree-1 convection.

## 4. Discussion

### 4.1. Phase Transitions

[47] An endothermic phase change would be expected to promote long-wavelength structures in the mantle. While such a phase transition is a partial barrier to convection [Christensen and Yuen, 1985], it is more effective at suppressing flow at shorter wavelengths [Tackley *et al.*, 1993]. Studies performed with an isoviscous sub-lithospheric mantle demonstrate this effect [Tackley *et al.*, 1993; Harder and Christensen, 1996; Harder, 2000]. In the Earth, the spinel-perovskite transition occurs at a depth of 670 km. On Mars, this transition occurs very close to the CMB if it occurs

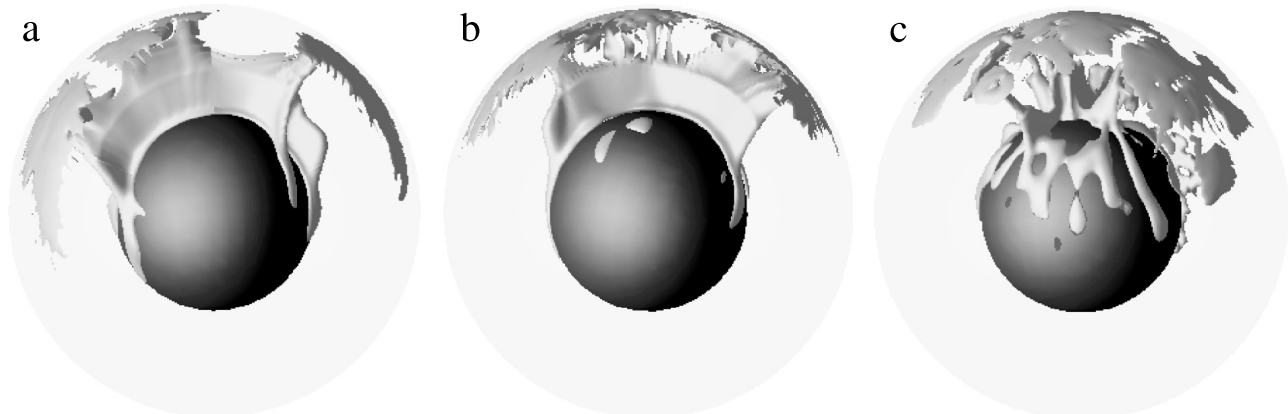


**Figure 8.** Temperature structures for cases with reduced internal heating. Upwellings, with residual temperature = 0.03 (a) for case V4 at 240 My, (b) for case V5 at 254 My, and (c) for case V6 at 273 My. Downwellings are omitted for clarity.

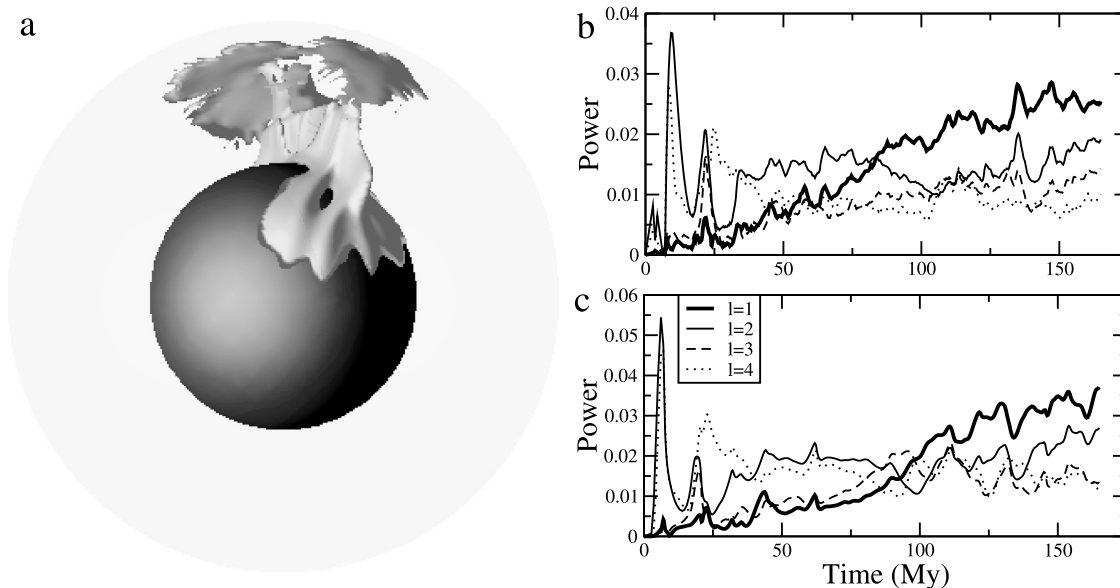


**Figure 9.** Temperature structures for case V7 with increased  $Ra$ . (a) Upwellings at 110 My with residual temperature = 0.05. Spectrum (b) at 110 km depth and (c) at 1670 km depth.

at all. Even with a relatively small radius of 1400 km for the core, the transition occurs only 120 km above the CMB. This puts the transition in the lower thermal boundary layer of the mantle; the region responsible for plume formation. The phase transition may inhibit the formation of small-scale plumes and allow only the largest ones to form. This results in a mantle dominated by a single large upwelling. Our cases P1 and P2 show this pattern (Figures 1a and 1b) and support the earlier work [Harder and Christensen, 1996; Harder, 2000].

[48] When a moderate temperature dependence is used as in case P3, the convective pattern looks much different (Figure 1c). The precise reason for this is not well understood. Tackley [1996] indicated that the radial dependence of viscosity that arises from temperature dependence (and other factors) is the dominant control on the planform of convection. However, our cases P3 and P4 have remarkably different convective planforms (Figures 1c and 2a), despite having the same radial viscosity profiles (Figure 1e). Our results suggest that lateral variations in viscosity have important effects on convective planform particularly when they occur in the boundary layer.

[49] This study has identified a number of difficulties in using phase transitions to generate degree-1 convection in Mars' mantle. First, the mantle viscosity is believed to be strongly temperature dependent [Karato and Wu, 1993; Karato and Jung, 2003]. However, we are only able to produce a degree-1 pattern using a constant or weakly temperature-dependent viscosity ( $E \leq 50$  kJ/mol). Second, the timescale required to develop this pattern is inconsistent with the timescale of the formation of the crustal dichotomy [Frey, 2004]. It takes about 5 Gy to form a single-plume structure. Attempts to reduce this time by raising the convective vigor or  $Ra$  resulted in a shorter-wavelength structure with an increased number of plumes (Figure 3). Finally, there is also doubt as to the existence of the

endothermic phase transition in the Martian mantle. A recent study of Mars' moment of inertia indicates that the planet's core is sufficiently large that the perovskite phase may never occur [Yoder *et al.*, 2003]. Our results suggest that the phase change may not be an effective way of producing degree-1 convection in the Martian mantle.

#### 4.2. Viscosity Layering

[50] Viscosity layering tends to have a reddening effect on the spectrum of convective structures [Zhang and Yuen, 1995; Bunge *et al.*, 1996]. This effect has been used to generate degree-1 convection in the Martian mantle [Zhong and Zuber, 2001]. The precise physical reason for this is not well understood. A Rayleigh-Taylor stability analysis [Zhong and Zuber, 2001] indicates that  $\ell = 1$  is the most unstable wavelength, when a factor of  $\sim 100$  viscosity jump is present in the midmantle. The energetics of convective systems indicate that for a layered mantle viscosity, convection at long wavelengths is more efficient at removing heat from the mantle, and depending on the size of the viscosity jump, the system may evolve toward a state of degree-1 convection [Lenardic *et al.*, 2006].

[51] Pressure dependence causes the viscosity to increase with depth, promoting the formation of long wavelengths. However, purely temperature- and depth-dependent viscosity models (e.g., case V1) failed to produce a degree-1 structure. Case V3, which included a factor of 25 viscosity jump successfully produced a degree-1 upwelling with the same overall viscosity contrast as in case V1. Case V2 with a factor of 8 jump has roughly equal power at degrees 1 and 2. Thus we observe a progression of increasing power at degree-1 as the size of the viscosity jump increases, as illustrated by Figures 5a–5c. A strong (factor of 25) jump forms a one-plume degree-1 structure, a weak (factor of 8) jump forms a ridge-like degree-1 structure, and the absence of a jump causes a degree-2 pattern to develop.

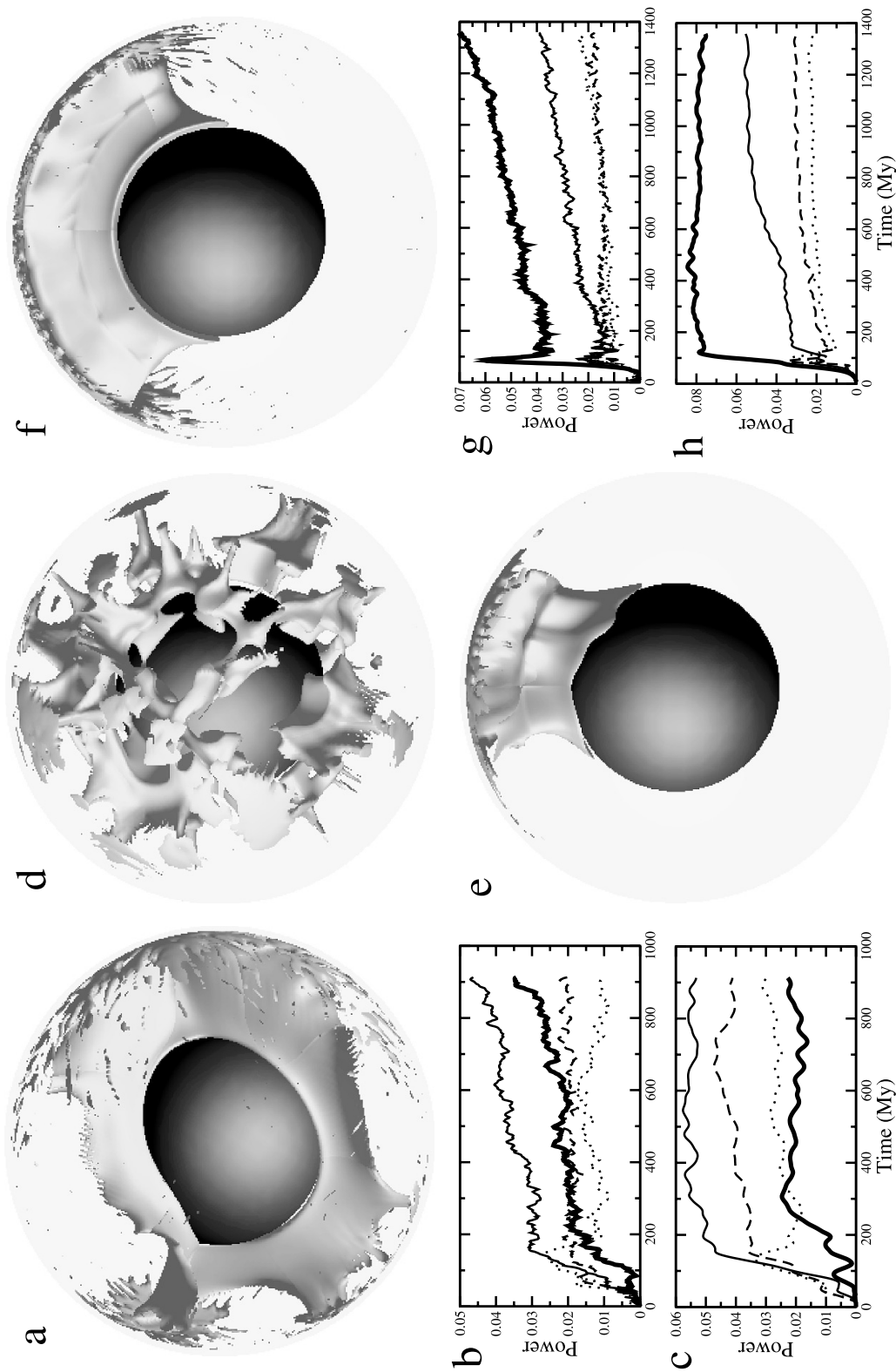


**Figure 10.** Temperature structures for cases with high activation volume. (a) Upwellings for case V8 after 900 My with residual temperature = 0.03. Time-dependent spectra of temperature structures in case V8 at the first four spherical harmonics (b) at a depth of 110 km and (c) at a depth of 1670 km. Here  $\ell = 1-4$  are represented by thick solid, thin solid, dashed, and dotted lines, respectively. Evolution of temperature structures for case V10 with residual temperature = 0.02 (d) at 67 My, (e) at 161 My, and (f) at 888 My. Spectrum of temperature structures in case V10 at the first four harmonics (g) at a depth of 110 km and (h) at a depth of 1670 km.

[52] The required viscosity structure with a jump of a factor of 8 or higher to generate degree-1 convection is consistent with the Earth's mantle rheology and viscosity [Karato and Wu, 1993; Hager and Richards, 1989]. This required viscosity jump is also significantly less than the factor of 500 of Zhong and Zuber [2001] from 2-D models. This viscosity jump is not necessarily a discontinuity, but rather a change in viscosity with depth more rapidly than pressure dependence would account for. A viscosity jump of a factor of 30 in the Earth's upper mantle is consistent with geoid models [Hager and Richards, 1989]. This depth may correspond to the transition from dislocation creep to diffusion creep that may take place in the Earth's upper mantle [Karato and Wu, 1993]. Owing to Mars' lower gravity, a similar feature would occur in the midmantle. A rapid change in effective viscosity associated with this transition might be expected. Such a rapid change in viscosity might also be attributable to an early magma ocean that may have melted the planet down to about this depth. Partial melt remaining from this magma ocean may still be present throughout the Noachian, reducing the effective upper mantle viscosity [Elkins-Tanton *et al.*, 2003].

[53] How rapidly a degree-1 structure can form is important for understanding the crustal dichotomy, given that the dichotomy may have formed in the early Noachian or earlier [Frey *et al.*, 2002; Nimmo and Tanaka, 2005; Solomon *et al.*, 2005]. Case V3 forms a degree-1 upwelling within about 175 My after the start of the calculation. We observe no significant dependence of the convective planform on the convective vigor, or  $Ra$ . Increasing  $Ra$  (i.e., reducing viscosity) helped the degree-1 pattern to emerge more quickly. Case V7, with  $Ra$  8 times larger than case V3, forms a degree-1 structure after 98 My (Figure 9). This timescale is appropriate to the formation of the crustal dichotomy. Solomon *et al.* [2005] suggested that the dichotomy may have formed at planetary formation of 4.5 Ga based on geochemical mass balance arguments and that the Rayleigh-Taylor overturn of magma ocean residue [Elkins-Tanton *et al.*, 2003, 2005] is the only mechanism that can operate on this fast timescale. Our calculations show that depending on viscosity, mantle convection can also lead to rapid formation of degree-1 structure. In fact, this viscosity-dependent timescale is similar to that in the overturn of magma ocean residue. Parmentier *et al.* [2002] showed that the overturn of magma ocean residue may take  $\approx 500$  My in order to produce the lunar mare basalts. This overturn timescale can be reduced by lowering the mantle viscosity and by increasing the thickness of the residue layer [Parmentier *et al.*, 2002].

[54] Degree-1 convection from our models, once formed, can be maintained over hundreds of My. We think that this long-lived degree-1 mantle convection is essential in maintaining the crustal dichotomy after its formation. The dichotomy formed during the earliest stage of Martian history, when the crust and mantle were still quite warm and weak. Long-wavelength topographic features on such a body tend to relax on the timescale of 100 My [Nimmo and Stevenson, 2001; Zuber *et al.*, 2000; Roberts and Zhong, 2005]. Without being maintained in some way, the crustal dichotomy would have vanished long before the present. This may have implications for other formation mechanisms

for the dichotomy. For example, if rapid overturn of magma ocean residue produces the dichotomy at 4.5 Ga [Solomon *et al.*, 2005], it is unclear how the crustal dichotomy may be maintained. This is because the residue material should rest on the CMB after the overturn and should not excite any significant degree-1 mantle flow.

[55] The models presented here are for stagnant-lid convection. It has been suggested that early Mars may have been in a sluggish-lid regime, making it easier to thicken the crust above the plume. Other studies suggest that it may be easier to develop degree-1 convection beneath a sluggish lid [Breuer *et al.*, 1997], than under a stagnant lid, suggesting that our results should hold up in that environment. Our models have an internal heating rate ranging between about 46 and 92%. This internal heating includes contributions from both radiogenic heating and secular cooling of the mantle. We find that the results are rather insensitive to the rate of internal heating. Cases V3, V5, and V6, with internal heating rates from 46 to 85% all produce degree-1 convection. The degree-1 structure in case V6, with the smallest internal heating rate consists of multiple plumes, rather than one (Figure 8c). This is because the large temperature drop at the bottom thermal boundary favors plume formation. These results are contrary to mobile-lid convection, in which a very high fraction ( $\approx 85\%$ ) of internal heating is needed to generate significant power at  $\ell = 1$  [McNamara and Zhong, 2005].

[56] The internal heating rate can be related to the CMB heat flux that may be potentially constrained by the existence of a global magnetic field early in Martian history. Global CMB heat flux on the order of a few terawatts is required to drive the geodynamo [Buffett, 2002]. Our models are able to produce CMB heat fluxes consistent with this estimate. We expect that the CMB heat flux in Mars was close to this limit, given that it shut down fairly early [Nimmo and Stevenson, 2000]. This suggests that a relatively large fraction of the mantle's heat was produced internally, consistent with an early primordial mantle, when the cooling of the mantle is rather rapid and before crustal formation has depleted it of much of the radiogenic elements.

[57] While this study has demonstrated the feasibility of generating degree-1 convection on a short timescale, we acknowledge that it does not guarantee the formation of the crustal dichotomy from it. In particular, the crust should be included, given that the dichotomy is largely a variation in crustal thickness. Modeling the crust requires the inclusion of a separate chemical layer, and is beyond the scope of this study. This is a topic for future work. Zhong and Zuber [2001] mentioned two mechanisms by which the degree-1 convection may lead to the dichotomy: melt forming in the plume head and erosion of the base of the crust over the upwelling. In the first scenario, the additional crust that formed in the southern hemisphere would have cooled in the presence of the early magnetic field and been magnetized [Arkani-Hamed, 2003]. This is consistent with MGS observations of strong magnetic anomalies on the southern highlands, and a relative dearth of such features on the northern plains [Connerney *et al.*, 2001]. While detailed modeling of the melt production has not been done, it is reasonable to assume that a degree-1 plume would produce

crust in a similar pattern, and maintain a largely degree-1 shape for the crustal dichotomy.

## 5. Conclusions

[58] We have examined two mechanisms of generating degree-1 convection in the Martian mantle, endothermic phase changes, and layered viscosity, using numerical models with different convective vigor, heating, and rheological parameters in both 2-D-axisymmetric and 3-D spherical geometry. Our main results can be summarized as follows.

[59] 1. An endothermic phase transition near the CMB may promote the formation of degree-1 convection, if the mantle viscosity is constant or weakly temperature dependent, but not with a more realistic rheology, with activation energy greater than 100 kJ/mol. In these models with degree-1 structure, this pattern takes billions of years to develop, and increasing the convective vigor results in a shorter-wavelength structure with a greater number of plumes rather than the hastening of degree-1 generation. On the basis of these results, we think that phase changes are not an effective way of producing the crustal dichotomy and long-wavelength structures on Mars.

[60] 2. For models that include fully temperature- and pressure-dependent viscosity, we find that an overall sublithospheric radial viscosity variation of a factor of 100, including a factor of 8–25 jump in the midmantle is sufficient to produce degree-1 convection. The time required to develop degree-1 convection from our models ranges from 100 My to several hundred My, depending inversely on the vigor of convection. This timescale is consistent with the formation of the crustal dichotomy. The rate of internal heating does not affect the formation of a degree-1 structure for the range of 46 to 92% internal heating that we examined in this study. Degree-1 convection produced by layered viscosity models plays an important role in not only producing the crustal dichotomy, but also maintaining it.

[61] 3. There is often good agreement between 2-D axisymmetric and 3-D models. However, when they differ, it is always easier to produce degree-1 in 3-D than in 2-D. Strongly pressure-dependent viscosity tends to produce ridge-shaped upwellings, whereas a viscosity profile with a shallower pressure gradient forms more classical plumes.

[62] **Acknowledgments.** This research is supported by NASA grant NNG05GM11G, the David and Lucile Packard Foundation, and the Alfred P. Sloan Foundation. We thank Adrian Lenardic and David Stegman for their careful reviews.

## References

Arkani-Hamed, J. (2003), Thermoremanent magnetization of the Martian lithosphere, *J. Geophys. Res.*, *108*(E10), 5114, doi:10.1029/2003JE002049.

Breuer, D., D. A. Yuen, and T. Spohn (1997), Phase transitions in the Martian mantle: Implications for partially layered convection, *Earth Planet. Sci. Lett.*, *148*, 457–469.

Buffett, B. A. (2002), Estimates of heat flow in the deep mantle based on power requirements for the geodynamo, *Geophys. Res. Lett.*, *29*(12), 1566, doi:10.1029/2001GL014649.

Bunge, H.-P., M. A. Richards, and J. R. Baumgardner (1996), Effect of depth-dependent viscosity on the planform of mantle convection, *Nature*, *379*, 436–438.

Christensen, U. R., and D. A. Yuen (1985), Layered convection induced by phase transitions, *J. Geophys. Res.*, *90*, 291–300.

Connerney, J. E. P., M. H. Acuña, P. J. Wasilewski, G. Kletetschka, N. F. Ness, H. Réme, R. P. Lin, and D. L. Mitchell (2001), The global magnetic field of Mars and implications for crustal evolution, *Geophys. Res. Lett.*, *28*, 4015–4018.

Elkins-Tanton, L. T., E. M. Parmentier, and P. C. Hess (2003), Magma ocean fractional crystallization and cumulate overturn in terrestrial planets: Implications for Mars, *Meteorol. Planet. Sci.*, *38*, 1753–1771.

Elkins-Tanton, L. T., S. E. Zaranek, E. M. Parmentier, and P. C. Hess (2005), Early magnetic field and magmatic activity on Mars from magma ocean cumulate overturn, *Earth Planet. Sci. Lett.*, *236*, 1–12.

Frey, H. V. (2004), A timescale for major events in early Mars crustal evolution, *Lunar Planet. Sci. Conf.*, XXXV, abstract 1382.

Frey, H. V., and R. A. Schultz (1988), Large impact basins and the mega-impact origin for the crustal dichotomy on Mars, *Geophys. Res. Lett.*, *15*, 229–232.

Frey, H. V., J. H. Roark, K. M. Shockey, E. L. Frey, and S. H. E. Sakimoto (2002), Ancient lowlands on Mars, *Geophys. Res. Lett.*, *29*(10), 1384, doi:10.1029/2001GL013832.

Hager, B. H., and M. A. Richards (1989), Long-wavelength variations in Earth's geoid: Physical models and dynamical implications, *Philos. Trans. R. Soc., Ser. A*, *328*, 309–327.

Halliday, A. N., H. Wanke, J. L. Birck, and R. N. Clayton (2001), The accretion, composition, and early differentiation of Mars, *Space Sci. Rev.*, *96*, 197–230.

Harder, H. (2000), Mantle convection and the dynamic geoid of Mars, *Geophys. Res. Lett.*, *27*, 301–304.

Harder, H., and U. R. Christensen (1996), A one-plume model of Martian mantle convection, *Nature*, *380*, 507–509.

Hartmann, W. K. (1973), Martian surface and crust: Review and synthesis, *Icarus*, *19*, 550–575.

Karato, S., and H. Jung (2003), Effects of pressure on high-temperature dislocation creep in olivine, *Philos. Mag.*, *83*, 401–414.

Karato, S., and P. Wu (1993), Rheology of the upper mantle: A synthesis, *Science*, *260*, 771–778.

King, S. D., and G. Masters (1992), An inversion for radial viscosity structure using seismic tomography, *Geophys. Res. Lett.*, *19*, 1551–1554.

Lenardic, A., F. Nimmo, and L. Moresi (2004), Growth of the hemispheric dichotomy and the cessation of plate tectonics on Mars, *Earth Planet. Sci. Lett.*, *222*, 807–817.

Lenardic, A., M. A. Richards, and F. H. Busse (2006), Depth-dependent rheology and the horizontal length-scale of mantle convection, *J. Geophys. Res.*, doi:10.1029/2005JB003639, in press.

McGill, G. E., and A. M. Dimitriou (1990), Origin of the Martian global dichotomy by crustal thinning in the Late Noachian or early Hesperian, *J. Geophys. Res.*, *95*, 12,595–12,605.

McNamara, A. K., and S. Zhong (2005), Degree-one mantle convection: Dependence on internal heating and temperature-dependent rheology, *Geophys. Res. Lett.*, *32*, L01301, doi:10.1029/2004GL021082.

Neumann, G. A., M. T. Zuber, M. A. Wieczorek, P. J. McGovern, F. G. Lemoine, and D. E. Smith (2004), Crustal structure of Mars from gravity and topography, *J. Geophys. Res.*, *109*, E08002, doi:10.1029/2004JE002262.

Nimmo, F., and D. J. Stevenson (2000), Influence of early plate tectonics on the thermal evolution and magnetic field of Mars, *J. Geophys. Res.*, *105*, 11,969–11,979.

Nimmo, F., and D. J. Stevenson (2001), Estimates of Martian crustal thickness from viscous relaxation of topography, *J. Geophys. Res.*, *106*, 5085–5098.

Nimmo, F., and K. Tanaka (2005), Early crustal evolution of Mars, *Annu. Rev. Earth Planet. Sci.*, *33*, 133–161.

Norman, M. D. (1999), Thickness and composition of the Martian crust estimated from rare earth elements and neodymium-isotopic compositions of Martian meteorites, *Meteorit. Planet. Sci.*, *34*, 439–449.

Parmentier, E. M., S. Zhong, and M. T. Zuber (2002), Gravitational differentiation due to initial chemical stratification: Origin of lunar asymmetry by the creep of dense KREEP, *Earth Planet. Sci. Lett.*, *201*, 473–480.

Roberts, J. H., and S. Zhong (2004), Plume-induced topography and geoid anomalies and their implications for the Tharsis Rise on Mars, *J. Geophys. Res.*, *109*, E03009, doi:10.1029/2003JE002226.

Roberts, J. H., and S. Zhong (2005), Crustal relaxation and its implications for the Martian crustal dichotomy, *Lunar Planet. Sci. Conf.*, XXXVI, abstract 2170.

Sleep, N. H. (1994), Martian plate tectonics, *J. Geophys. Res.*, *99*, 9327–9343.

Solomon, S. C., et al. (2005), New perspectives on ancient Mars, *Science*, *307*, 1214–1220.

Tackley, P. J. (1996), Effects of strongly variable viscosity on three-dimensional compressible convection in planetary mantles, *J. Geophys. Res.*, *101*, 3311–3332.

- Tackley, P. J., D. J. Stevenson, G. A. Glatzmaier, and G. Schubert (1993), Effects of an endothermic phase transition at 670 km in a spherical model of convection in the Earth's mantle, *Nature*, *361*, 699–703.
- Tanaka, K. L., D. H. Scott, and R. Greeley (1992), Global stratigraphy, in *Mars*, edited by H. H. Kieffer et al., pp. 354–382, Univ. of Ariz. Press, Tucson.
- Turcotte, D. L., and G. Schubert (2002), *Geodynamics*, 2nd ed., 456 pp., Cambridge Univ. Press, New York.
- Wieczorek, M. A., and M. T. Zuber (2004), Thickness of the Martian crust: Improved constraints from geoid-to-topography ratios, *J. Geophys. Res.*, *109*, E01009, doi:10.1029/2003JE002153.
- Wilhelms, D. E., and S. W. Squyres (1984), The Martian hemispheric dichotomy may be due to a giant impact, *Nature*, *309*, 138–140.
- Wise, D. U., M. P. Golombek, and G. E. McGill (1979), Tectonic evolution of Mars, *J. Geophys. Res.*, *84*, 7934–7939.
- Yoder, C. F., A. S. Konopliv, D. N. Yuan, E. M. Standish, and W. M. Folkner (2003), Fluid core size of Mars from detection of the solar tide, *Science*, *300*, 299–303.
- Zhang, S., and D. A. Yuen (1995), The influence of lower mantle viscosity stratification on 3-D spherical-shell mantle convection, *Earth Planet. Sci. Lett.*, *132*, 157–166.
- Zhong, S. (2002), Effects of lithosphere on the long-wavelength gravity anomalies and their implications for the formation of the Tharsis rise on Mars, *J. Geophys. Res.*, *107*(E7), 5054, doi:10.1029/2001JE001589.
- Zhong, S., and M. T. Zuber (2001), Degree-1 mantle convection and the crustal dichotomy on Mars, *Earth Planet. Sci. Lett.*, *189*, 75–84.
- Zhong, S., M. T. Zuber, L. Moresi, and M. Gurnis (2000), Role of temperature-dependent viscosity and surface plates in spherical shell models of mantle convection, *J. Geophys. Res.*, *105*, 11,063–11,082.
- Zuber, M. T., et al. (2000), Internal structure and early thermal evolution of Mars from Mars Global Surveyor topography and gravity, *Science*, *287*, 1788–1793.
- 
- J. H. Roberts, Department of Astrophysical and Planetary Sciences, University of Colorado, UCB 391, Boulder, CO 80309-0391, USA. (jhr@anquetil.colorado.edu)
- S. Zhong, Department of Physics, University of Colorado, UCB 390, Boulder, CO 80309-0390, USA. (szhong@anquetil.colorado.edu)